Chapter 2

Computational models of heart pumping efficiencies based on contraction waves in spiral elastic bands

2.1 Introduction

The human heart is well known as a mechanical pumping device of amazing efficiency, but we do not completely understand it. But it is not widely recognized how simple are the questions for which we do not know the conclusive answers. Here is one example: Myofibrils can contract by at most 15% [16]. If we imagine, for the sake of estimate, that myofibrils surround the heart as planar loops, then a simple geometrical argument suggests that with circumference contracting to 0.85 of its length, the surrounded cross-sectional area, and, therefore, the internal volume contracts to $(0.85)^2 \approx 0.72$, i.e., by at most 28%. This estimate is in a stark contrast with the physiologically well known fact that at each beat the healthy heart ejects blood in the amount of above 50% of the left ventricle volume. Thus, there is a glaring paradox between the physiologically possible contraction of myofibrils and physiologically realized ejection fraction.

Biological pumping organs, including the heart, are complex multi-scale systems. The function of the heart involves intricate physiological, biochemical, biophysical, cytological, hydrodynamical and many other aspects [15]. We would like to emphasize that all these aspects, however important, cannot resolve the above mentioned simple geometrical paradox. Indeed, whatever happens on the cell scale and on a smaller scale, whatever happens on the scale of microns, cannot resolve the contradiction between the amount of myofibril contraction and volume ejection on the scale of several centimeters.

An important progress in understanding this problem was achieved in paper by Sallin [41]. It was shown by a geometrical argument that helical arrangement of fibers, as a matter of principle,

can help resolve this paradox. Indeed this way of thinking was launched by the discovery of helical arrangements of fibers in histological studies [20]. The helical arrangements have also been confirmed by more recent MRI studies [22]. However, it remains unknown how specifically the helical arrangement is used by nature to resolve the efficiency issue in the heart. One of the reasons for this uncertainty is that MRI used in work [22] does not differentiate the muscle fibers from inactive fibers, showing a very complicated network of helical fibers.

One of the approaches to understanding heart mechanics is through modeling. For the purpose of simulations, the complex arrangement of the helical fibers requires simplification. The most popular simplification is based on the idea that the myocardium is a series of shells that contain helical fibers with changing angles of orientation. Very significant resources are directed at modeling the heart with a variety of approaches, sometimes with a very hight degree of computational sophistication [42, 43, 46]. Most of these models simply ignore the physiological constraint on the maximum myofibril contractility and assume that fibrils can contract by any desirable amount. In some such models, authors simply take the physiological ejection faction as an input parameter [46]; as a result the strain in the fibers is much greater than possible in nature. Other models, while never taxing the contractile ability of the fibers, never achieve the physiological ejection fraction, instead focusing on other aspects of heart function [45, 51].

We believe that the key to resolving the pumping efficiency paradox is not just in the helical arrangement of the myofibrils, but in the way these helical myofibrils bundle together. At about the same time that the helical fibers were discovered, another histological study found that the muscle fibers seem to be arranged in a single bundle in the shape of a double helix [21, 55]. Recently, through new imaging techniques this histological evidence has been given more weight. Modern MRI technology, such as DTMRI, illuminate the actin in the muscle cells, thus imaging exclusively the muscle fibers instead of a combination of muscle and other tissues [23]. These images show a bundled arrangement that is closer to a one double helical muscle band configuration then to the popular shell model. Our goal in this chapter is to demonstrate how double helical arrangement of the myofibrils explains the physiologically achieved volume ejection fraction without overstraining the fibrils.

Helically arranged fibrils can also be seen in the images of embryonic fish hearts [5–7] where, however, overall geometry is much simpler – in the early stages of development the entire heart can be thought of as a cylinder surrounded by the helical fibrils. For the sake of comparison, we will reproduce all our model calculations for this simpler geometry.

For our purpose, the model does not require too many details, there is no need to incorporate any microscopic features, they only matter in determining the phenomenological parameters of our large scale model. Additionally, among the decisive simplifications we do not have to take explicit account of blood hydrodynamics.

We model the myocardium as an elastic band. The material of the band becomes active when it is excited, which can generate volume forces in its body. As a corner stone of our simulations we specify that at maximal excitation the material contracts by 15% in the direction of the fibers. Despite a long standing knowledge of the Purkinje network that excites the adult heart, the timing of the cardiac muscle response to excitation is still unclear [16]. To get around this issue we assume a simple linear response to excitation, but vary the excitation patterns in our simulations.

Besides checking the performance of our "model hearts" as pumps we also pay close attention to their dynamics. The dynamics of the adult heart is very important to its proper function [56]. Indeed the twist of the left ventricle can be used to judge the relative health of the heart [27–29]. Part of the reason twisting is so important is that it is used as a spring mechanism for rapid refilling. As a result the dynamics are more complicated than simply turning one way with the contraction and the other with the relaxation. There is a qualitative jerkiness to the twisting motion of the heart that can be seen in open heart surgeries. We use the existence of the twist as an benchmark to the appropriateness of the excitation pattern we pick.

The plan of this chapter is as follows. In section 2.2, we formulate our model in greater detail, and explain how we choose the values of its parameters. We also describe our way of computational implementation of this model and data analysis. In section 2.3, we concentrate on the results obtained using our model. First, we demonstrate the adult heart model's ability to reach physiological maximal ejection fractions under the simplest of excitation schemes. Second, we show that there is no dynamical twist in either of the two models of the adult heart and embryonic tube heart in response to a step or a temporal wave excitation. Third, we find that the spatio-temporal wave excitation patterns are able to overcome this barrier without loosing the pumping efficiency. We conclude with the discussion and outlook in section 2.4.

2.2   Methods

2.2.1   Geometries of muscle bands

Fibers in both the adult and embryonic heart form a complex matrix. In our models, we simplify this complexity by taking into account only the dominant bundles of the muscle fibers. To model the muscle fiber bundle it is necessary to know where it is in space and how it is oriented. We choose to describe this mathematically. To do so, we specify the centerline of the bundle. This centerline can be thought of as a single fiber, around which all of the other fibers will bundle. The shape of the centerline is roughly determined by averaged orientation of all fibers of the dominant bundle. Here, we mathematically describe the centerline using parametric equations in cylindrical coordinates-$[\theta, r, z]$, where we choose the circumferential coordinate (polar angle), θ, to be the parameter.

Once the centerline is determined, we describe the rest of the bundle by specifying the other

fibers to run parallel to the centerline: For every θ the new fiber is at a constant distance from the centerline at the same θ. To make sure that the new fibers do not cross, this is done by stepping away from the centerline in a direction that is perpendicular to the tangent of the centerline. In this work the muscle bundles we model have the shape of bands, meaning that the thickness of the bundle is much smaller than either the length or the width of the bundle. In our models, bands enclose pumping chambers by surrounding them with their wider side; that means the bands are orientated in such a way that the thickness is always taken to be in the radial direction. And the 3D band geometry is described in cartesian coordinates, $[x, y, z]$, with three parameters, θ along the length of the band, ξ along the width, and ζ in the thickness direction.

2.2.1.1   A simple tube

One of the simplest chambers we can enclose with a band is a tube. The fibers can be arranged circumferentially or longitudinally, or they could form a spiral about the tube. There are many examples in nature where there is a helical muscle structure, ranging from worms to embryonic fish hearts [5, 10, 57]. Such muscle bands can be easily described by a set of parametric equations. In cylindrical coordinates, $[\theta, r, z]$, the centerline of the spiral band is defined such that radius, r, is a constant, while z grows linearly with θ:

$$r = R , \qquad z = R\theta \cot \alpha , \tag{2.1}$$

where α is the pitch (fiber) angle, and R is the radius of the cylinder. The polar angle θ parameterizes the curve and ranges, $0 \leq \theta < \theta_{max}$.

As it is known from differential geometry, the orientation of the centerline determines in each point a triplet of mutually orthogonal vectors (called Frenet vectors), namely tangent, normal, and binormal [58]. In our case, normal vector everywhere points in r direction away from the cylinder, while tangent vector and binormal vector have no r components and lie on the surface of the band, and their other components are given by:

$$t_\theta = \sin \alpha , \qquad t_z = -\cos \alpha , \qquad n_\theta = -\cos \alpha , \qquad n_z = -\sin \alpha . \tag{2.2}$$

Based on the known equations for the centerline and its binormal, we can define a surface of a spiral band by simply stepping away by a small length along the binormal from the centerline. The thickness of the band is given by small variations in the constant R. The parameterized description of the 3D spiral with fiber angle α are then given in cartesian coordinates by:

$$z = r\theta \cot \alpha + \xi n_z; \; x = (R + \zeta) \cos (\theta + \xi n_\theta); \; y = (R + \zeta) \sin (\theta + \xi n_\theta). \tag{2.3}$$

The variables ξ and ζ identify the position within the band in the direction of width and thickness, respectively. These variable change in the range $-w/2 < \xi < w/2$ and $0 < \zeta < t$, where w and t width and thickness, respectively. The constants R, α, and θ_{max}, allow us to specify which parameters (cylinder radius, cylinder length, fiber length, cylinder volume) are to be kept constant. Different configurations of the spirals used in this work are shown in figure 2.1.
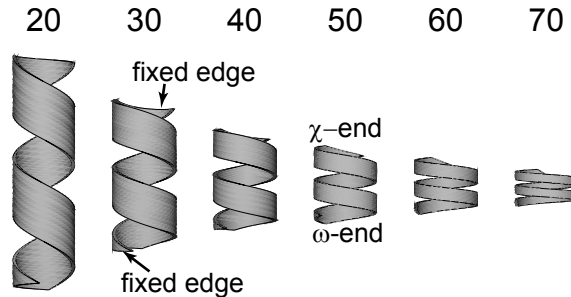

Figure 2.1: Images of the spiral muscle band models for the embryonic heart. The numbers indicate the pitch (fiber) angle, $\alpha = 20°$, $30°$, $40°$, $50°$, $60°$, $70°$ are shown. For all the spirals shown here the radius of the tube is constant. The length of the band is also constant, and as a result the length of the tube varies with the pitch angle. The width of the band is taken to be half of the value that would have fully covering the surface of the tube, and as a result the width varies with the pitch angle. The edges that are fixed during simulations are shown on the spiral of $\alpha = 30°$. On the spiral $\alpha = 50°$ the ends of the tube are labeled corresponding to the start of spatial contractions at $\chi-$end, and the end of contraction at the $\omega-$end.

2.2.1.2   A two chamber structure

The adult human heart is a more complex structure than a tube, but its chambers are also bound by helical fibers. In order to explain our way of modeling this structure, let us first define the same nomenclature as used in heart physiology. There are two pumping chambers, the left and right ventricles. We can crudely describe the left ventricular volume as bounded by the left pulmonary surface on the outside of the heart and the septum on the inside. Likewise, the right ventricular volume is bound by the septum on the inside of the heart, and the anterior (sternocostal) surface on the outside. Importantly, this structure is not axisymmetric. In other words, when we introduce the z-axis, along the long-axis of the heart, directed from the apex to the center of the basal plane, it does not imply any rotational symmetry.

We describe the ventricular surfaces by introducing the polar angle θ in the horizontal plane perpendicular to the z-axis. For the left ventricular surface, we assume that its cross-section by the vertical plane going through the z-axis at any θ represents a parabola, $z = ar^2$, with parabola vertex at the heart apex, but with different, θ dependent coefficient: $a = a(\theta)$. Although the left ventricular surface is not completely axisymmetric, it looks roughly like a paraboloid, which means variations of $a(\theta)$ are not large throughout the closed surface, for $0 \leq \theta \leq 2\pi$. Part of this surface

represents the left pulmonary surface, while the other part - septum. Adjacent to the septum part, on its outer side, there is another surface, significantly more curved, which represents the anterior surface; it joins smoothly the left ventricle surface along the boundary of septum and left pulmonary surface, and extends significantly outwards in between (the latter means that, at the basal plane level, the horizontal distance from the long axis (or from the z-axis) to the middle of anterior surface is significantly longer than the distance from long axis to the middle of the septum). We do not need to specify any mathematical description of the anterior surface, because we do not plan to address the right ventricular volume. For simplicity, we will refer in this chapter to the left and right ventricular chambers shapes as non-axisymmetric paraboloid and half-paraboloid, respectively. The surfaces of the ventricular chambers can be seen as part of our model in figure 2.2A. In the heart these surfaces are formed by the fibers of the myocardium.
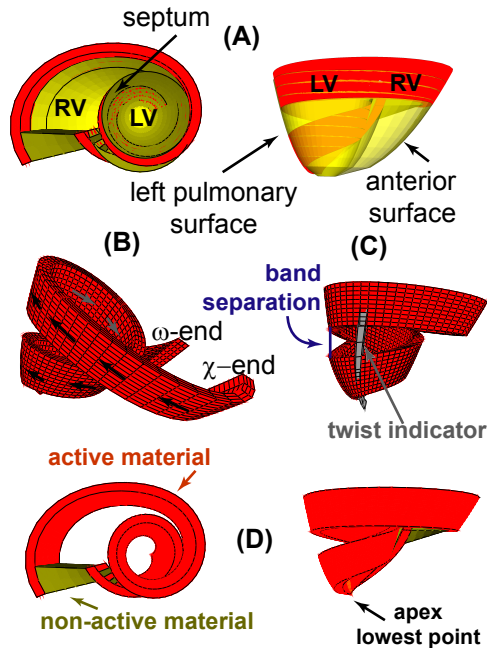

Figure 2.2: Initial band shape and fitted volume shown from different points of view. (A) The chambers for left ventricles (LV) and right ventricle (RV) are drawn in yellow. The left pulmonary and anterior surfaces, and the septum are indicated. The left ventricle is in the shape of a non-axisymmetric paraboloid, and the right ventricle is a half-paraboloid. The model band is shown in red on the surfaces of LV and RV. (B) The proposed double helix band is shown with the fiber angle indicated by the arrows. The ends of the band are labeled corresponding to the start of spatial contractions at χ−end, and the end of contraction at the ω−end. (C) The double helix band is shown from the back, with the separation between the loops indicated. This separation was picked, such that at minimum long-axis of the left ventricle the band would not impinge on itself. The soft material of the twist indicator is shown in grey. (D) The band in different orientation, with labeled active and nonactive material, as well as the apex of the heart. The non-active material that connects the two ends of the band is fixed in the horizontal plane, while the apex is fixed vertically.

There is histological evidence that the fibers are arranged in a spiral band, as shown by Torrent-

Guasp [21], who postulated that the heart muscle is a single band that starts from the pulmonary aorta, hugs the right ventricle, winds down to the apex, as the descending segment, and then spirals up to the aortic valve as the ascending segment. To mathematically describe this intertwined double helix we took the original physical model created by Torrent-Guasp and approximated its shape with mathematical equations. It is, of course, more complicated in terms of mathematical presentation than a simple spiral. Theretofore, as a first step we describe the orientation of the fibers by specifying the long-axis coordinate, z_{cent}, as a function of polar coordinate θ for the centerline:

$$z_{cent} = C_1 - C_2 \frac{\theta^{A_1}}{A_2} \exp\left[-\frac{\theta}{B_2}\right] \tag{2.4}$$

where C_1, C_2, A_1, A_2, B_2 are constants. The polar coordinate θ varies $\theta_{max} \geq \theta \geq 0$, where θ_{max} corresponds to the start of the band at the pulmonary aorta, and $\theta = 0$ corresponds to the end of the ascending segment. This interpolation formula is designed such that at large θ the change in z is dominated by the exponential factor, thus describing the fibers hugging the right ventricle; at small θ, z decreases sharply due to the power law factor θ^{A_1}, thus describing the ascending segment; at the cross-over range of θ the interplay between these two factors describes the descending segment.

The r-coordinate of the centerline should now be constructed in such a way that the centerline correctly skirts the ventricular surfaces, the non-axisymmetric paraboloid and half-paraboloid, which we discussed a few lines back. The simplest idea would be to take just the paraboloid $r_{\text{cent}} = \sqrt{(z_{\text{cent}} + C_3)/a}$, with some constant a (C_3 determines the position of 0 on the z-axis). However, we should keep in mind that the band and, therefore, its centerline in the adult heart has to make two turns around the heart's long-axis. That means, θ will have to change over the interval significantly longer than one full turn of 2π. Therefore, for the centerline skirting the paraboloid, there will inevitably be two points with the same r and the same z, corresponding to angles θ_{crossing} and $\theta_{\text{crossing}} + 2\pi$; and this will mean the physically meaningless self-overlap of the band at $\theta_{\text{crossing}} = \pi\left(-1 + \cot\frac{\pi}{A_1 B_2}\right)$. To avoid this self-overlap, we force the radii at these two points to be different by introducing the Factor 1 which bends the centerline away from self-crossing. We also introduce Factor 2 , which is only significant in the region of anterior surface and describes the fact that this surface bends significantly outwards from the septum. An illustration of the resultant shape of the band if Factor 1 and Factor 2 were not included can be found in appendix D figure D.1. We choose the middle of anterior surface to correspond to $\theta_{\text{right}} = 3.8\pi$ and write:

$$
\begin{aligned}
r_{cent} &= \sqrt{z_{cent} + C_3}\,[\text{Factor 1}]\,[\text{Factor 2}], \\
\text{Factor 1} &= 1 + C_4 \cos\left(\frac{\theta - \theta_{crossing}}{2}\right), \\
\text{Factor 2} &= 1 + C_5 \exp\left(-(\theta - \theta_{right})^2\right),
\end{aligned}
\tag{2.5}
$$

where, C_3, C_4 and C_5 are constants. The constants of equations 2.4 and 2.5 are not independent when related to the geometry of the heart.

To make the mathematical description of the 3D shape of the band simpler, we approximate the direction of the width to be along the z-axis. The parameterized three dimensional structure is then described in cartesian coordinate, (x, y, z), by:

$$z = z_{cent} + \xi, \qquad r = \sqrt{z + C_3} \, [\text{Factor 1}] \, [\text{Factor 2}] + \zeta, \tag{2.6}$$
$$x = r \cos \theta, \qquad y = r \sin \theta,$$

where $-w/2 < \xi < w/2$ and $0 < \zeta < t$, with w and t are the width and the thickness of the band, respectively. The resulting structure can be seen in figure 2.2B.

2.2.2 Choosing the Geometrical Parameters

In both models, embryonic and adult heart, there is a range of parameters that can be varied. Some of the parameters were specified during the mathematical formulation of the model, others we varied in different simulations. We base the choice of parameters on physiological observations, the goals of the simulations, and computational needs.

2.2.2.1 Embryonic tube heart

Pitch angle: It is not possible to extract the pitch angle (fiber angle) from the images of the embryonic heart. We therefore wanted the ability to vary the fiber angle. In the experiments the angle is varied between $5° \le \alpha \le 85°$.

Radius of the tube: In the embryonic heart model the radius of the tube is known. Thus, we chose to keep the radius of the tube constant, namely $R = 0.25$ cm.

Number of turns: From the available images it is unclear how far up the tube the spiral fibers extend. Therefore we base our choice for the number of turns on the adult heart model – this ensures that the two models are easier to compare to each other. As a result, we specify for the spiral to make two full turns. In these simulations we specify it to go around another quarter of a turn, so that the boundaries do not impact the main body of the spiral. Therefore, $\theta_{max} = 4.5\pi$.

Length of the tube: Once the number of turns of the spiral, the radius, and the pitch angle are specified, the length of the tube is mathematically determined: $\{\text{Length}\} = \theta_{max} R \tan \alpha$.

Fiber length: Once the above parameters are chosen the fiber length is determined:
$\{\text{Fiber Length}\} = \theta_{max} R / \cos \alpha$.

Band width: The choice of the above parameters also defines the width of the band necessary to cover the whole surface of the tube. We chose for the width of the band to be limited to half of what would cover the tube, to insure that the material did not impinge on itself during twisting: $w = 0.25\pi r \cos\alpha$.

Band thickness: The thickness of the band is constant and small compared to the width:
$t = 0.02$cm.

2.2.2.2 Adult heart

Unlike the constants that described the shape of the spiral the constants in equations 2.4-2.6 are given by a complicated relationship with physical quantities, so we will present their values where they first occur.

Number of turns: This parameter is dictated to be two turns by the histological evidence. This places the limit on θ_{max} to be 4π. We extend this a little to connect the two ends of the band: $\theta_{max} = 4.08\pi$.

Long axis dimension: The long axis dimension is taken to be the same as in the normal adult heart, about 7 cm. Therefore, in equation 2.4 the constat $C_2 = 7$.

Fiber angle: Unlike the pitch angle of the simple spiral, the fiber angle is not constant in the double helical arrangement. We took the information from the histological studies done by Torrent-Guasp [17, 21]. The fiber angle dictates the formulation of equation 2.4 and the values for the other constants are: $C_1 = 4.9$, $A_1 = 1.3$, $A_2 = 0.5$, $B_2 = 2$. The fiber orientation differences in the thickness of the myocardium at the crossing point dictates that in equation 2.5 the constant $C_4 = 1/6$. The fiber orientation at the apex is also dictated by the position of the vertex on the long axis: $C_3 = -0.77$.

Basal radius: The basal radius of the left ventricle is taken to be the same as in the adult heart, about 3.5 cm. This is also inherent in the parameters described above.

Right heart size: The parameter controlling the size of the right heart, was estimated so that the fitted right ventricle volume would correspond to the volume in a normal adult heart (about 130 mL): $C_5 = 1$ in equation 2.5.

Band width: To ease computation the band width is assumed to be a constant. The width is chosen ($w \approx 2.5$ cm) such that the bottom of the mitral left segment does not impinge on the top of the descending segment during maximal contraction. The separation between the two parts of the band are shown in figure 2.2C.

Band thickness: The thickness of the band is constant and small compared to the width

$(t \approx 0.5 \text{ cm})$.

2.2.3 Material properties

The properties of the material of the organ's muscle are inevitably dictated by the muscles building blocks – muscle cells. The muscle fibers contract along the length of the fiber, thus the muscle band, which consists of a group of parallel muscle fibers, will contract in the same direction. The cells cannot contract over 15%, and thus the band will not exceed this maximum shortening ratio at any point along its length. To conserve volume, while it is shortening in the fiber direction the band will expand in the other two. The band can contract as a whole, or parts of it can shorten independently of each other. That means that the cells can act separately along the length of the fiber and the fibers in the width of the band can contract at different times from each other. For simplicity, we assume a linear elastic response while the material is not excited. The material is incompressible, so the maximal computationally possible Poisson ratio is chosen, $\nu = 0.48$ (an ideal incompressible material has $\nu = 0.5$). The only forces in these models are those produced by the active material, so we choose to normalize all the stresses by the Young's modulus, E_Y, of the muscle fiber. Therefore, the Young's modulus for any material included in the model is described in terms of E_Y of the active material.

As regards to the structure of the adult heart, it would have been impossible to model the double helix without the band coming into contact with itself. Indeed, in some areas of the ventricles the interaction between the material with different fiber direction is very important as illustrated by other works [46]. It was, therefore, necessary to insert a few pieces of the collagen matrix, a non-active material, to make the model applicable. The non-active material was chosen to be four times softer then the active material, i.e., the Young's modulus of the non-active material is one fourth of the Young's modulus of the active material. One piece of collagen is placed at the cross over point connecting the band at $\theta_{crossing}$ and $\theta_{crossing} + 2\pi$. The other piece is used to connect the two ends of the band, i.e., between $\theta = 0$ and $\theta = 4\pi$. The collagen pieces are labeled in figure 2.2D in green.

2.2.4 Boundary conditions

Our models are not part of a whole organism, so there is no vasculature to hold them in place. It is, therefore, necessary for us to fix them in space, otherwise in response to the force produced by excitation, the structure will gain acceleration and fly away. To do that we need to constrain at least three degrees of freedom.

2.2.4.1   Embryonic tube heart

We found that the most meaningful behavior is obtained by fixing both ends of the tube (shown in figure 2.1 for 30° pitch angle). This allows us to consistently look at pumping in a range of different contraction schemes. If only one end of the tube is fixed, the other flaps about, which makes it hard to determine the internal volume.

2.2.4.2   Adult heart

In order to easily compare the medical data on heart twist to the dynamics of our model, we wanted to fix the model in space by the same rules as are observed in nature. In the body, the top of the heart does not rotate, while the heart's apex does not move up or down. Therefore, the band structure is fixed in the horizontal plane by restraining the non-active material in the x-y-directions, in the same manner as the heart is constrained by the vessels. The lowest point of the double helix is assumed to be the apex, and is constrained in the vertical z-direction (figure 2.2D).

2.2.5   Different Excitation schemes

To begin with, let us consider what happens to the active material when it is excited. In the language of solid mechanics the deformation of the band will be described in terms of strains, ε, along the fiber direction and in both perpendicular directions. Since maximal contraction in response to excitation is 15%, the minimum strain in response to activation would be -0.15. We express the strains in response to excitation as $\varepsilon_{fiber}^{\text{Ex}} = 0.15\text{Ex}$ in the fiber direction and in both perpendicular directions as $\varepsilon_{perpend}^{\text{Ex}} = -0.085\text{Ex}$. Here, the excitation factor, Ex ranges between 0 for no excitation and -1 for a full excitation. If the structure is constrained the activation will induce stress. For example in the fiber direction the stress of a fully constrained structure would be $\sigma_{fiber} = E_Y \left(\varepsilon_{fiber} - \varepsilon_{fiber}^{\text{Ex}} \right)$, where ε_{fiber} is the total strain in the fiber direction. This means that the excitation factor, Ex, is the only input which activates the model, and drives its deformation.

The simplest dynamic scheme is to excite all the cells at the same time and have the fibers contracting in sync – making a uniform contraction. We also apply a wave-type excitation to our models. Of course, in creating waves there are a lot of degrees of freedom. We can change the duration of the excitation, the length of the wave, the origin point of excitation, etc. For a band, some of the simpler waves would be one dimensional. To ease the explanation let us label one end of the band χ and the other ω (these are labeled on figure 2.1 for pitch angle 40° and in figure 2.2B). A one dimensional contraction wave would then be described as originating from end χ of the band and traveling to end ω. This means that all the elements in width and thickness, the ones at the same centerline natural coordinate, will contract and relax together. For ease of comparison to the uniform contraction, where all the elements are contracted together, we create a wave that has the

contraction front traveling from end χ of the band to end ω. Once the contraction front reaches the ω end of the band, the relaxation front starts from the original χ end. This means that there is one instance of time where the whole band is contracted. To contrast this long wave, we also run a simulation where the wave is shorter and the relaxation front starts before the contraction front reaches the ω end. The excitation factor (Ex) is then dependent on both time, t, and the band coordinate, s, and can be approximated by the following piece-wise linear interpolation:

$$\text{Ex}(s,t) = \begin{cases} 0 & : \quad t < t_1 \\ \frac{-(t-t_1)}{t_2-t_1} & : \quad t_1 \leq t < t_2 \\ -1 & : \quad t_2 \leq t < t_3 \\ \frac{-(t_4-t)}{t_4-t_3} & : \quad t_3 \leq t < t_4 \\ 0 & : \quad t \geq t_4 \end{cases} \tag{2.7}$$

$$t_1 = \frac{L_1}{s_{max}}x, \quad t_2 = \frac{L_1}{s_{max}}x + T_1, \quad t_3 = \frac{L_2}{s_{max}}x + T_2, \quad t_4 = \frac{L_2}{s_{max}}x + T_3,$$

where s_{max} is the length of the band, and L_1, L_2, T_1, T_2, T_3 are constants that determine the shape of the excitation wave. Figure 2.3 shows a graphical representation of the excitation patterns used in this work. The x-axis on this plot shows the coordinate on the band, s. End χ is considered the origin at zero, and end ω is the end of the band at 100% of the bands length (s_{max}). The y-axis shows time. To read one of these contour plots, you can draw a horizontal line at the time of interest, then at each point on the band you will find a color that represents the degree of contraction (blue - contracted, red - relaxed). The following is a description of each excitation pattern and the constants corresponding to it:

Step excitation: For a uniform contraction $L_1 = L_2 = 0$, and thus there would be no dependance on the spatial variable. The other constants were taken to be $T_1 = 0.4$ sec, $T_2 = 0.7$ sec, $T_3 = 1$ sec. See the contour plot for this wave in particular in figure 2.3A.

Long spatial wave excitation: For the full band length wave the constants are $L_1 = L_2 = s_{max}$, $T_1 = 0.005$ sec, $T_2 = 0.45$ sec, $T_3 = 0.5$ sec. See the contour plot for this wave in particular in figure 2.3D.

Medium spatial wave excitation: For a spatial wave shorter than a full band length the constants are $L_1 = L_2 = 1.2s_{max}$, $T_1 = 0.005$ sec, $T_2 = 0.375$ sec, $T_3 = 0.4$ sec. See the contour plot for this wave in particular in figure 2.3C.

Shifted long wave excitation: For the shifted long wave the constants are $L_1 = 0.4s_{max}, L_2 = 0.95s_{max}$, $T_1 = 0.005$ sec, $T_2 = 0.275$ sec, $T_3 = 0.325$ sec. See the contour plot for this wave in particular in figure 2.3E.
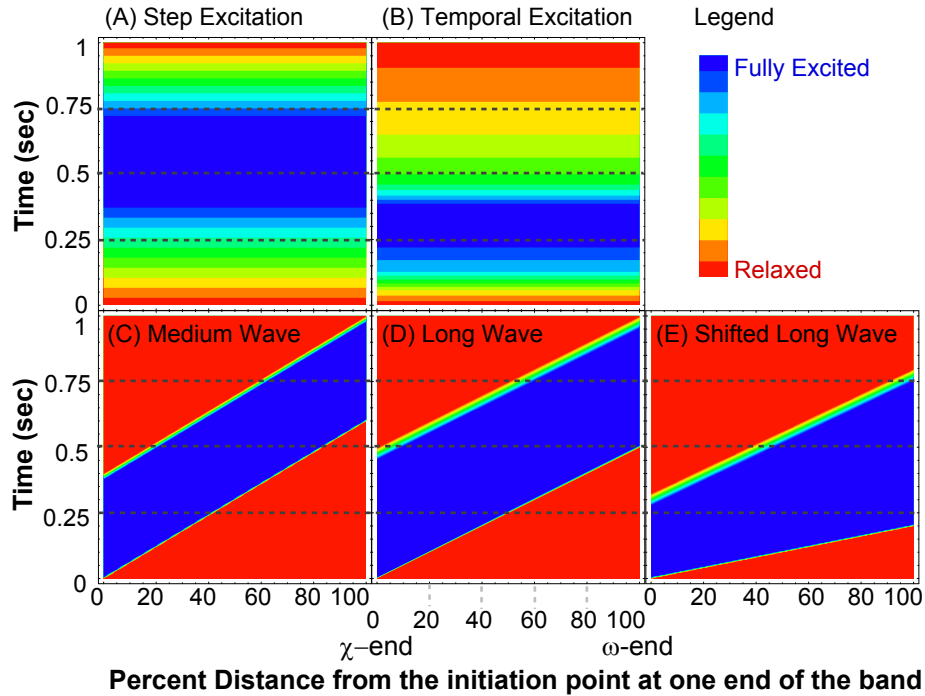
Figure 2.3: Parametric plots for five excitation waves. To read these plots follow a horizontal lines, at a time of interest, the color at the position of the band indicates the contraction state. The scale at the top right corner shows the legend with red-relaxed and blue-fully contracted. At the top are plots for uniform excitation schemes, where the whole band contracts at once. At the bottom are plots of spatial wave excitation schemes, where the excitation wave starts at $\chi-$end of the band and travels to the $\omega-$end of the band. (A) A step excitation, with the whole band being excited rapidly, and held at the fully excited state for 0.5 seconds. (B) A temporal excitation, with the whole band excited gradually - mirroring the change in volume of the physiological left ventricle. (C) Medium Wave, the band is never contracted all at once. (D) Long Wave, at $0.5s$ the band is fully contracted. (E) Shifted Long Wave, the speed of the excitation and relaxation fronts are adjusted, such that the full excitation occurs earlier $(0.25s)$.

Temporal excitation: For the temporal wave, there was no dependance on time, and the activation was described by a table with linear approximations between values. See the contour plot for this wave in particular in figure 2.3B.

Time (sec)	Excitation
0	0
0.055	−0.25
0.09	−0.50
0.13	−0.75
0.225	−0.938
0.375	−1
0.415	−0.75
0.47	−0.50
0.545	−0.375
0.66	−0.25
0.83	−0.125
1	0

2.2.6 Computational methods

To enable spatio-temporal excitation it is necessary to allow different parts of the band to contract independently. This creates a complex coupling between local small deformations and large global shape responses, making it a challenging modeling problem. Another difficulty is that we are considering three dimensional geometries. To combat these problems, we utilize finite element analysis. It is possible, with small quadrilateral elements, to build very complicated shapes. The finite element method also breaks down a complicated problem of the dynamics of a complicated system in response to excitation into a set of manageable equations. Since this set is very large, it behooves us to use the computing power available to solve it. We therefore, model these bands using a finite element package, ABAQUS/Standard, designed to handle such problems. In the finite element code we use ABAQUS built in tools to independently "excite" each node, and when the nodes of an element are "excited," the element contracts in the longitudinal fiber direction.

Please note that the finite element formulation of these models forces the s band coordinate in equation 2.7 to be discreet. The effects that this has on the results can be easily seen by varying the number of elements along the band. However, with the large number of elements used here (over 3000), the effect is very small compared to the overall changes in the structure.

2.2.7 Data Analysis

In this work we do not model fluid. If the blood was included it would be necessary to add valves to the chamber. Otherwise, most of the blood pumped during a contraction would flow back during relaxation. As a result, the pump would be very ineffectual. Therefore, for our simulations we simply

assume that the valves are present. This assumption implies that if the volume of the chamber is increased, there will be blood sucked into the pump from the inlet. When the volume of the chamber is decreased, the blood is forced out through the outlet. Therefore, we can simply keep track of the volume that would fit inside the spiral to calculate the effectiveness of the pump.

For the purposes of calculating the volume, the results from the ABAQUS/Standard analysis were processed with Fortran and Matlab code. To define the bounding surface, we extract the position of each node of the inner surface of the band for each time step. For the embryonic model the pumping chamber in its initial state is approximated as a cylinder. Although during the deformation the radius of the chamber varies with the z-coordinate, the chamber as a whole can still be approximated as a figure of revolution. When considering finite elements we view every small layer dz as a cylinder. The volume of the whole chamber is then the sum of the volume of all these cylinders.

For the adult heart model, the double helical band, the left ventricle volume was described in section 2.2.1.2. We assume that this general description of the left ventricular chamber as a non-axisymmetric paraboloid is valid throughout the deformation. Therefore, as the chamber deforms, the parabolic parameter $a(\theta)$ changes. In finite element formulation the chamber is broken into small polar sections of $d\theta$. Each slice is bounded by a piece of paraboloid and two vertical planes intersecting at the long-axis. The volume of the left ventricle is calculated by adding the volumes of each of the $d\theta$ slices.

To measure the pumping, volume reduction, efficiency of the pumps we calculate the ejection fraction, EF. For the tubular model we use a generic formula:

$$\text{EF(t)} = \frac{V_{\text{max}} - V(t)}{V_{\text{max}}}, \qquad \text{and} \qquad \text{EF}_{\text{max}} = \frac{V_{\text{max}} - V_{\text{min}}}{V_{\text{max}}}, \tag{2.8}$$

where, $V(t)$, V_{max} and V_{min} are the volume at time t, maximum volume and minimum volume of the chamber, respectively. For the adult heart model we use the same formulation as is used in the medical field:

$$\text{EF(t)} = \frac{V_{\text{initial}} - V(t)}{V_{\text{initial}}}, \qquad \text{and} \qquad \text{EF}_{\text{max}} = \frac{V_{\text{initial}} - V_{\text{min}}}{V_{\text{initial}}}, \tag{2.9}$$

where, $V(t)$, $V_{initial}$ and V_{min} are the volume at time t, initial volume and minimum volume of the chamber, respectively. Note, that the initial volume is the end-diastolic volume, and the minimum volume is the end-systolic volume.

We use ABAQUS/CAE to look at the dynamical aspects of the simulations. To ease the visual comparison we fix a strip of material to the outside of the left ventricle. The strip is made from a very soft elastic non-active material (Young's modulus two orders of magnitude less than that of the other inactive material). As a result the strip has no effect on the deformation of the structure

as a whole. The presence of twist can be judged by the deformation of this strip, like temperature is judged by the use of a thermometer. Initially the strip of material is in an $r - z-$plane. During the contraction of the chamber the long-axis shortens, as a result the deformation of the strip will always have a component in the plane. If the strips deforms out of the plane there is twist in the left ventricle. If during deformation it remains in the plane there is no twist.

To look at the dynamical aspects of the embryonic model we include an outline of the original configuration for comparison. As a result it is possible to see changes in pitch angle, i.e., twist.

2.3   Results

In this work we look at two types of models - a double helical adult heart model and a simple spiral embryonic tube model. Each model is subject to different excitation schemes. For the embryonic heart there is very little data for comparison. Indeed, while, it has been found that there are helical fibers in the embryonic heart tube, there is no data for the pumping efficiency under different conditions. By contrast, for the adult heart there is a large volume of data for comparison with the model results. Consequently, we guide our exploration of both models, by comparing the adult heart model results with medical data.

	Contraction Type				
	Physiological	Step	Uniform Temporal	Medium Spatial Wave	Long Spatial Wave
EF_{max}	50%-60%	54%	54%	53%	54%

Table 2.1: The ejection fraction values for double helical pumps under different excitation patterns

2.3.1   Step excitation

In considering helical structures let us begin with looking at the simplest possible excitation scheme – a step excitation. In this scheme the whole band is excited at once, leading to an immediate contraction of all elements.

We first looked at how the double helical adult heart model responds to this type of excitation. Table 2.3 shows the maximal ejection fraction for this type of contraction. In this case the maximum ejection fraction is 54%. This is well in the range of normal physiological values of $50\% - 60\%$. However, as can be seen in the plot of figure 2.4A, in a step contraction the volume changes in a completely different manner from the physiological. As a consequence, it is unsurprising that the dynamics of the left ventricle in this model has no visible twist. This effect is illustrated in the snapshots of the simulations in figure 2.5. We next looked at how the tubular model was affected. Like in the adult heart model there is no visible twist (figure 2.6). In figure 2.7 the maximal ejection
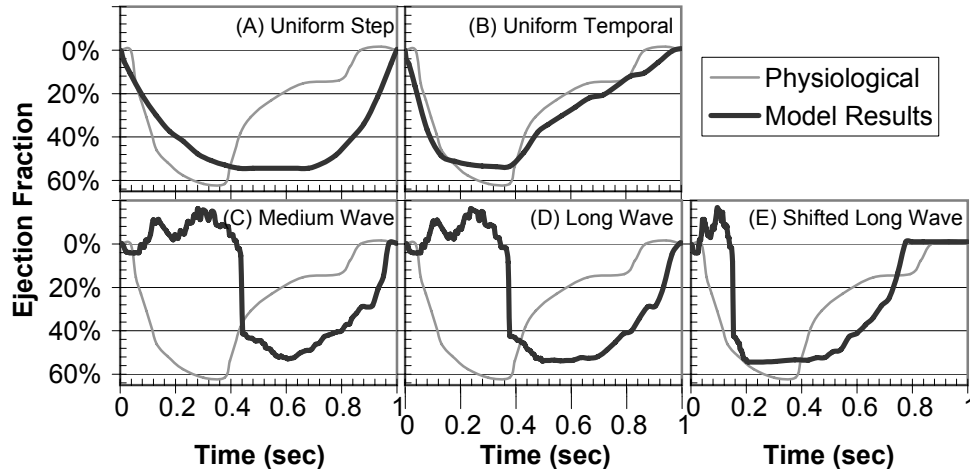
Figure 2.4: The left ventricular ejection fraction vs. time for adult heart model subject to different excitation patterns. The ideal physiological data taken from [15] is drawn in grey for comparison with model data in black. (A) Uniform Step excitation: the maximal ejection fraction is sufficiently close to physiological, but the speed with which it increases and decreased is completely different from physiological. (B) Temporal excitation: Both the maximal ejection fraction and the shape of the response are close to ideal physiological. (C, D) Medium and Long spatial waves: The maximal ejection fraction matches physiological needs, but it occurs at 0.6s instead of 0.38s. The shape is different, with the initial increase in volume, and the initiation of pumping at 0.4s. The medium wave response has more rapid filling than the long wave. (E) The shifted long wave: The maximal ejection fraction timing is shifted quite close to physiological.

fraction as a function of pitch angle for this excitation pattern is shown in dark blue. These results never top the 28% that would be possible with circumferential fibers. The only surprise is that at very low pitch angles the ejection fraction starts to increase instead of going to zero as we expected (see appendix A.1 for analytical calculations for non-helical fibers). This happens because in these models the fiber length and θ_{max} are kept constant. As a result for pitch angles below 20° the length of the tube is so much larger than the radius that the structure buckles in the middle to reduce stress, making the volume appear larger. This effect is unlikely to be of any biological significance, because in reality the muscle band is encased in a collagen matrix.

2.3.2 Temporal excitation

To fit the model's left ventricular ejection fraction evolution with time to the physiologically observed throughout the course of a beat, we apply a temporal excitation. In this activation scheme, the excitation factor is approximated directly from physiological data, $\mathrm{Ex(t)} \approx -\mathrm{EF^{physio}(t)}/\mathrm{EF^{physio}_{max}}$.

As a result, the maximal ejection fraction remains unchanged, at physiological value of 54%. The plots of the ejection fraction vs. time in figure 2.4 show that using this method we can reproduce how the left ventricular volume changes with time in real physiological experiment. However in the snapshots of the simulation no significant twist is visible (figure 2.5).
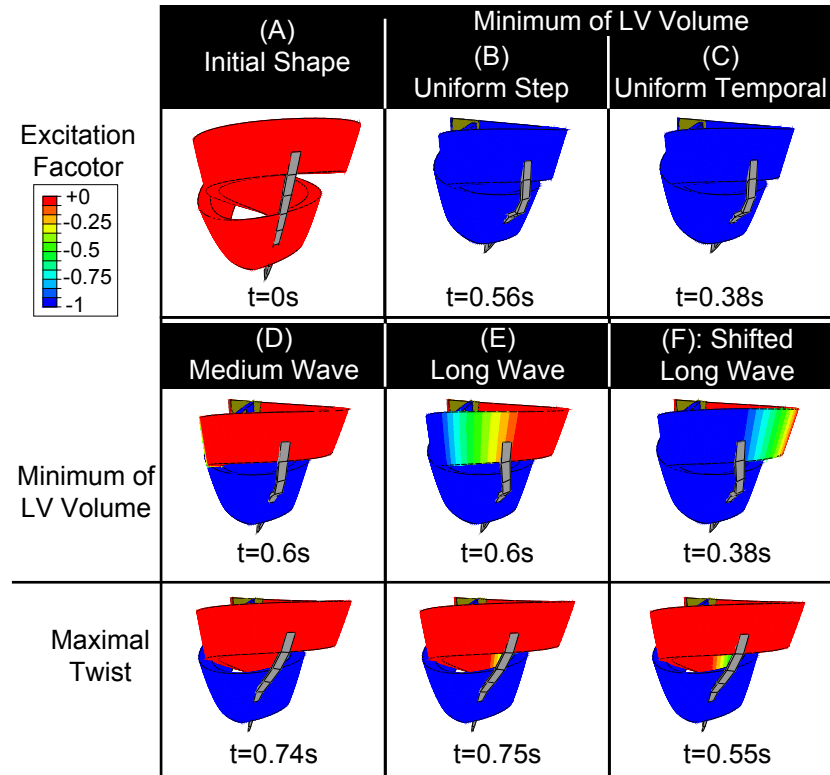
Figure 2.5: Snapshots of the movies for the adult heart model. The legend for the excitation factor is at the left (red-relaxed, blue-contracted). For each type of excitation discussed in this chapter we show the snapshots of the time at which LV volume was at a minimum. The presence of twist can be qualitatively judged by the out of plane deformation of the grey twist indicator. For the uniform excitation, no out of plane movements can be seen at any time. The models subject to the spatial excitation have twist indicator deformations out of plane. To showcase this, we provide another series of snapshots for the spatial wave excitations for times at which the twist was maximal (bottom panels).(A) Initial shape at time, $t = 0s$. (B) Uniform step: Minimum volume at t=0.56s. (C) Uniform temporal: Minimum volume at t=0.38s. (D) Medium wave: Minimum volume at t=0.6s; Maximal twist at t=0.74s. (E) Long wave: Minimum volume at t=0.6s; Maximal twist at t=0.75s. (F) Shifted long wave: Minimum volume at t=0.38s; Maximal twist at t=0.55s.

For a tube this type of excitation produced no significant differences in results when compared to the step excitation (shown in figure 2.7 in violet and blue). Any variations are slight and due to the time step - the time at which the maximal contraction occurs is in between sampled time steps. Figure 2.8 shows this difference between the response to the step and temporal excitations for a spiral with pitch angle of 60°, in blue and violet, respectively. Practically, the only difference in the response to the temporal excitation and the step excitation is in the timing. This makes sense, since the only variation we introduce for the temporal excitation is in the timing of the excitation. As a result it is unsurprising that, qualitatively, we cannot see any type of twist (figure 2.6).

To summarize, there are two problems with this type of contraction: First, we do not see any dynamic twist in the adult heart simulations, which we know is an integral part of a healthy heart.
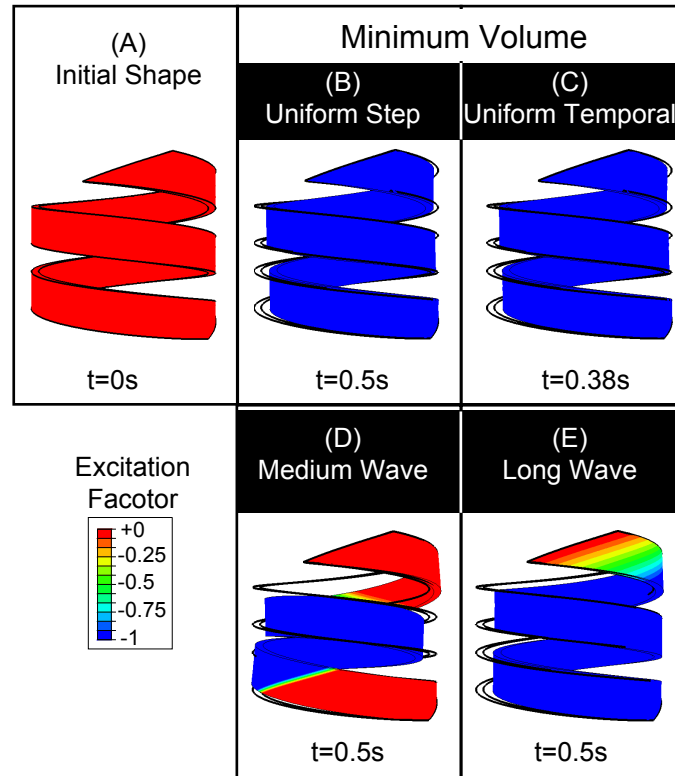
Figure 2.6: Snapshots of the movies for the embryonic heart model. The legend for the excitation factor is at the left on the bottom (red-relaxed, blue-contracted). For each type of excitation discussed in this chapter we show the snapshots of the time at which LV volume was at a minimum. The presence of twist can be qualitatively judged by comparing the initial band outline (thicker black lines) to the current shape. For the uniform excitation, no change in centerline angle can be seen at any time, i.e., only the radius of the spiral changes. The models subject to the spatial excitation have twist, which is indicated in the shift of the band away from the original outline. (A) Initial shape at time, $t = 0s$. (B) Uniform step: Minimum volume at t=0.5s. (C) Uniform temporal: Minimum volume at t=0.38s. (D) Medium wave: Minimum volume at t=0.5s (E) Long wave: Minimum volume at t=0.5s;

Second, this is an unrealistic type of contraction. In biology the muscles will either be excited or not; it is unlikely that a muscle cell would have such a complicated response to an excitation.

2.3.3 Spatial wave excitation

To resolve these problems we try a spatial wave excitation. For the purposes of this work we try a simple wave that starts at one end of the band and moves to the other, as described in section 2.2.5. A wave contraction is also very flexible in terms of easily imaginable compensation mechanisms available in case of damage.
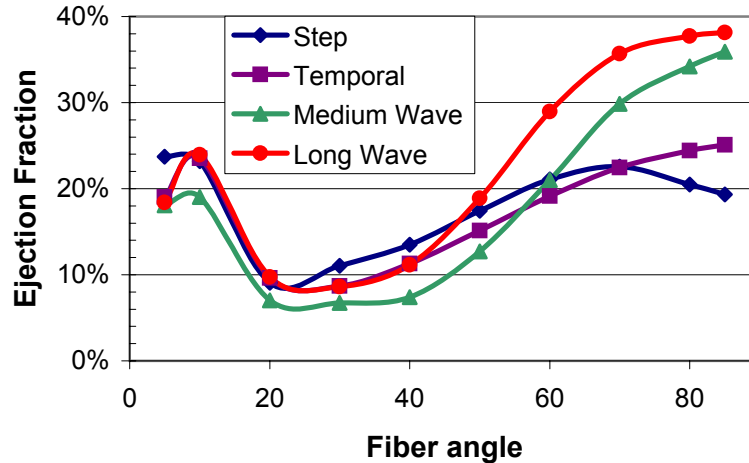
Figure 2.7: The dependence of the ejection fraction on the pitch angle for four different contraction schemes for a tube spiral geometry. Step excitation - blue, Temporal excitation - violet, Medium spatial wave - green, Long spatial wave - red. For pitch angles above $50°$ the spatial waves can achieve better ejection fractions than the uniform contractions. For pitch angles of $70°$ and above, it is possible to overcome the 30% ejection fraction possible with circumferential fibers.

2.3.3.1   Simple spatial waves: Adult Heart

The snapshots in figure 2.6 show that wave-type contractions produce a qualitatively visible twist. This twist, once calculated, can be used to judge independently from the volume-time relationship whether the excitation pattern is physiological. But how was the pumping ability affected?

The range of maximal ejection fractions for the adult heart model subject to different spatial wave contractions is $53\% - 54\%$, which is within the physiological range. Figure 2.4D show how this simple constant speed spatial wave excitations produces a complicated volume reduction response. We performed calculations for a broad range of values of the wave length $((L_2T_3 - L_1T_2)/s_{max}$ in equation 2.7 above). The ejection fraction results for the medium length wave (figure 2.4C), show that maximal ejection fraction was not impacted. In general, we found that the reduction in the length of the wave does not negatively impact the maximal ejection fraction until the wave is shorter than the portion of the band that defines the left ventricle. However, there are some significant differences between the responses of the model to the simple spatial wave excitations and physiological data, as we show and discuss below.

2.3.3.2   Timing of maximal contraction: Adult Heart

The simplest spatial excitation, the long wave, makes our model to respond in such a way, that the maximum ejection fraction is timed differently from the physiological response – it is late by 0.2 s. Obviously, this is caused by the speed of the contraction and relaxation wave fronts, which we chose arbitrarily. Thus, it is easy to fix by varying the speeds of the wave fronts. Figure 2.4E shows the

model response to a full length spatial wave with a different speed of the contraction and relaxation wave fronts (shifted long wave). In this case the maximal ejection fraction is timed quite closely to the physiological maximal contraction.

2.3.3.3   Initial increase in volume: Adult Heart

Another discrepancy between the model's response to the long wave excitation and the physiological behavior is that for the first $0.3s$ the volume increases from the diastolic value, which does not happen in a real heart (figures 2.4C, 2.4D). The initial increase in volume is due to the helical nature of the band. When one end of the band is activated, it pulls on the portion of the band that bounds the left ventricle, increasing its volume. Our preliminary results (not shown) indicate that this initial increase in volume can also be adjusted, or taken out altogether, by making the spatial wave a little more complicated.

2.3.3.4   Simple spatial waves: Tube

When the spatial waves are applied to the spiral of the embryonic heart model the results are surprising. Figure 2.7 shows the maximal ejection fraction as a function of fiber angle for the long and medium spatial waves in red and green, respectively. At some pitch angles, if a helical structure is combined with a wave-like contraction, it is possible to exceed the maximal ejection fraction of the uniform excitation. Additionally, it is possible to overcome the limit on maximal ejection fraction previously achieved only with circumferential fibers (appendix A.1). The possibility to achieve over 28% ejection fraction without contracting the entire band at once could be beneficial in nature where muscle fatigue comes into play. But what is the mechanism behind the higher efficiency?

2.3.3.5   Pumping with suction: Tube

The plot in figure 2.8 shows how the volume of the tube with the spiral subject to spatial wave excitations initially increases. This is in contrast to uniform excitations, which have no initial increase in volume. Note, that while the increase in volume is the same for both the long and medium spatial wave excitation, the long excitation achieves a smaller minimum volume. This happens because in both types of excitations initially the activated end of the band pulls open the other end. However, the long spatial excitation wave contracts the whole spiral, which in the end produces a larger contraction compared to the initial configuration.

Since we assumed that the valves were present, the effect of initial increase in volume creates suction. Thus, during the initial stages of the contraction the volume increases, leading to a higher change in volume overall. The mechanism for suction here is different from the one observed in embryonic fish hearts early in their development [5]. In paper [5], the embryonic hearts acted as an impedance pump. The impedance pumping that produces the suction is caused by the dynamical
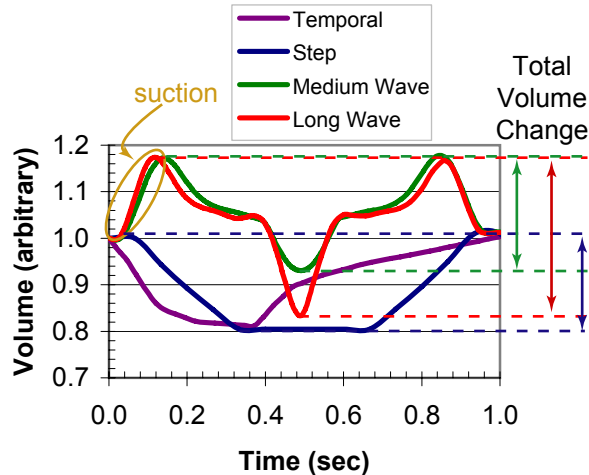
Figure 2.8: The volume evolution with time for four different excitation schemes applied to a spiral with a pitch angle of 60°. Step excitation - blue, Temporal excitation - violet, Medium spatial wave - green, Long spatial wave - red. The area where the volume is initially decreasing for models subject to spatial wave contractions is labeled as suction in yellow. The overall change in volume is indicated at the right. Here it is possible to see, that because of the suction effect the spirals driven by spatial wave excitations due a better job at pumping than the the spirals driven by uniform excitations.

movements of the spiral, which is seen in our model for most pitch angles with spatial excitation. At this point, it is impossible to know if the effect of suction from combining the helical nature of muscle fibers and a spatial wave excitation is used in embryonic pumping. It would be interesting to see what pitch angles the muscle fibers in the embryonic heart have and if the helical shape depends on the presence of valves.

2.4   Conclusions

Helical designs in living creatures are generally appreciated for their static structure, rather than the dynamics. In this respect, Torrent-Guasp model is distinct where a strong functional relationship between the heart's pumping function and its spiral muscle structure as a single band is proposed. By avoiding the complexity of modeling the whole structure at once, including all of the collagen and blood, we show that this simple band structure is akin to an engine behind the heart pumping action, for both a simple tube like the embryonic fish heart and a two ventricle pump.

In this work we have shown that it is possible to capture the adult's heart left ventricular volume evolution with time using a double helical model. This includes reproducing the maximal ejection fraction observed physiologically. The fact that we capture the maximal ejection fraction without overstraining the fibers is unique to this double helical model. However, this type of activation is biologically unrealistic and produces no dynamical twist of the left ventricle. Conversely, by activating this double helical structure with a spatial excitation, we can produce a visible left ventricular

twist without loosing our ability to capture the proper ejection fraction.

We have also shown that there is no benefit to helically arranged fibers in a tube-like embryonic heart unless the muscle cells are activated with a spatial wave excitation. This combination, also produces a dynamical twisting response, which might play a part in other pumping mechanisms.

By coupling this band like helical structures of the myocardium with a wave-like contraction schemes it is possible not only to exceed pumping efficiency expectations, but to take advantage of the dynamics such a system can provide. The beauty of this model is in its simplicity, which leads to great flexibility. We realize that a real cardiac system involves many factors on a lot of scale levels that have not been accounted for here, but because our model captures some of the important properties of these biological systems, such factors as the calcium excitation, the presence of different types of muscle cells, collagen, blood, and complicated excitation patterns, can now be treated as additions to the already constructed solid base.